Supporting Information for:

Domain-Like Ultra-Thin Layer Deposited Electrochemically from Carbazole-Functionalized PeryleneBisimide for Electron Collection in Inverted Photovoltaic Cells

Tao Feng,[b] Biao Xiao,[a] Ying Lv,[b] Zengqi Xie,*[a] Hongbin Wu,[a] Yuguang Ma*[a,b]

[a] Institute of Polymer Optoelectronic Materials and Devices
State Key Laboratory of Luminescent Materials and Devices
South China University of Technology
Guangzhou 510640, P. R. China
[b] State Key Laboratory of Supramolecular Structure and Materials
Jilin University, Changchun 130012, P. R. China

ygma@scut.edu.cn; msxiez@scut.edu.cn

Table of Contents:

1. Experimental Details and Synthesis

Materials and Methods: All reagents and solvents used for the synthesis were purchased from Aldrich and Acros companies and used without further purification. All reactions were performed under a dry nitrogen atmosphere. ^{1}H and ^{13}C NMR were recorded using a Bruker-300 spectrometer operating at 300 and 75 MHz in deuterated chloroform solution at 298 K. Chemical shifts were reported as δ values (ppm) relative to an internal tetramethylsilane (TMS) standard. UV-vis and fluorescence spectra were recorded on a Shimadzu UV-3600 spectro-photometer and a fluorospectrophomometer (Fluorolog-3) using 1 cm path length quartz cells, respectively. Cyclic voltammetry (CV) measurement was performed on a CHI600D electrochemical workstation with a glass-carbon disk electrode as the working electrode, a Pt wire as the counter electrode, Ag/Ag^+ non-aqueous electrode as the reference electrode and $TBAPF_6$ (0.1 M) in CH_2Cl_2 / acetonitrile (positive) or DMF (negative) as electrolyte. Atom force microscopy (AFM) measurement was carried out using a Digita Instrumental DI Multimode Nanoscope IIIa in taping mode.

Synthesis of *N*,*N′*-Bis(9,9-bis(6-(9H-carbazol-9-yl)hexyl)-9H-fluoren-2-ylphenyl)-1,7-bis(4-tert--butylphenoxy)perylene-3,4:9,10-tetracarboxdiimide (1)：*N*,*N′*-Bis(4-bromophenyl)-1,7-bis(4-tert-butylphenoxy)perylene-3,4:9,10-tetracarboxdiimide (116.2 mg, 0.115 mmol) and 9,9’-((2-(4,4,5,5-tetramethyl-1,3,2-dioxaborolan-2-yl)-9H-fluorene-9,9-diyl)bis(hexane-6,1-diyl))bis (9H-carbazole) (227.6 mg, 0.287 mmol）were added to a solution of K_2CO_3 (4.0 M) in a 15.00 mL : 2.50 mL : 2.50 mL (V/V/V) mixture of toluene/methanol/water. $Pd(PPh_3)_4$ (36.0 mg, 0.034 mmol) was used as the catalyst. The reaction mixture was stirred at 84 ℃ for 86 h under a nitrogen atmosphere. After cooling to room temperature, dichloromethane was added and the aqueous phase was extracted. The organic phase was collected and dried with anhydrous Na_2SO_4. After evaporation of the solvent, the residue was purified via chromatography by petroleum ether / dichloromethane 1:2 to yield a dark red solid (171.8 mg, 66%). ^{1}H NMR (300 MHz, $CDCl_3$, 293K, TMS): $\delta = 9.68$ (d, 2H; Ar-H), 8.66 (d, 2H; Ar-H), 8.40 (s, 2H; Ar-H), 8.04 (d, 8H; Ar-H), 7.73(m, 8H; Ar-H), 7.55 (d, 4H; Ar-H), 7.47(d, 4H; Ar-H),7.40 (m, 12H; Ar-H), 7.30 (m, 14H; Ar-H), 7.16 (m, 12H; Ar-H), 4.14 (t, 8H; CH_2), 1.93(m, 8H; CH_2),1.66(m, 8H; CH_2), 1.26 (s, 18H; CH_3),1.10 (m, 16H; CH_2), 0.65 ppm (m, 8H; CH_2); ^{13}C NMR (75 MHz, $CDCl_3$, 298K, TMS): 163.51, 163.13, 155.59, 152.48, 151.08, 150.70, 148.41, 142.12, 140.69, 140.62, 140.33, 139.25, 133.88, 133.75, 130.45, 129.42, 128.95, 128.11, 127.54, 126.98, 126.28, 125.52, 125.29, 124.00, 123.86, 122.73, 122.30, 121.61, 120.26, 119.93, 119.13, 118.63, 108.63, 55.00, 42.86, 40.32, 34.58, 31.96, 31.47, 29.73, 29.39, 28.77, 26.94, 26.86, 23.73, 22.72, 14.15 ppm; MS (MALDI-TOF): m/z: 2164.0 [M^+]; elemental analysis calcd (%) for $C_{154}H_{134}N_6O_6$: C 85.44, H 6.24, N 3.88, O 4.43; found: 85.66, H 6.68, N 3.65, O 4.01.

ECP Layer Deposition: The ITO-coated glass substrates were cleaned in an ultrasonic bath with toluene, acetone, ethanol, and deionized water, respectively, and then dried with nitrogen. The electrochemical polymerization was performed using a standard one-compartment, three-electrode electrochemical cell attached to a CHI 760D Electrochemical Workstation. An Ag/Ag^+ non-aqueous electrode was used as a reference electrode, ITO(~1 cm^2) was used as the working electrode, and titanium metal was used as the counter electrode (area: ~3 cm^2). A mixture of compound **1**, and $TBAPF_6$ (0.1 M) with CH_2Cl_2 and acetonitrile was used as the electrolyte solution. The electrochemical polymerization was processed by CV mode and after the electrochemical polymerization process, the resulting ECP layer was washed with a mixture of CH_2Cl_2 and acetonitrile (3:2, V:V), to remove any unreacted precursors and supporting electrolytes, and then dried with nitrogen. All measurements were carried out at room temperature under ambient conditions.

Inverted Polymer Solar Cells Fabrication: PCDTBT was purchased from 1-material Chemscitech Inc. (St-Laurent, Quebec, Canada) and used as received. The prototype PCDTBT:$PC_{71}BM$ inverted polymer solar cells were constructed as structure: ITO/ECL (X scanning cycles)/PCDTBT:$PC_{71}BM$ (90 nm)/MoO_3 (10 nm)/Al (100 nm). The PCDTBT:$PC_{71}BM$ (1:4 by weight) active blend layer with a thickness of 90 nm was prepared by spin-coating the chlorobenzene solution at 1000 rpm for 2 min. The MoO_3 and Al layers were formed by vacuum evaporation method. The background pressure of the chamber was under 10^{-6} Torr during the deposition process. The layer thickness of the deposited material was monitored *in situ* using an oscillating quartz thickness monitor. Power conversion efficiency values were determined from *J–V* curve measurements (using a Keithley 2400 source meter) under a 1 sun, AM 1.5G spectrum from a solar simulator (Oriel model 91192; 56 mW·cm^{-2}) in a glove box filled with nitrogen atmosphere (<1 ppm H_2O and <1 ppm O_2).

2. Synthetic route of compound 1

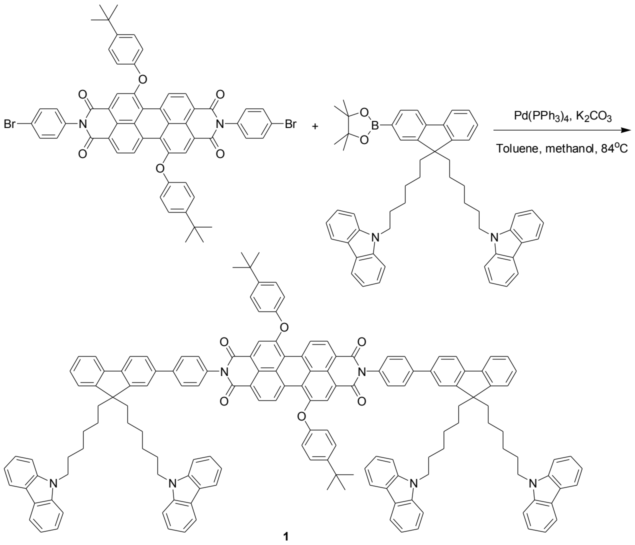

Scheme S1. Synthetic route of compound **1**.

3. Optical properties of compound 1

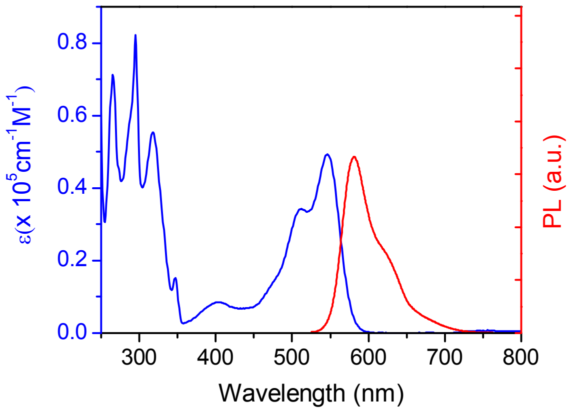

Figure S1. Absorption and PL spectra of compound **1** in dichloromethane (c = 1 × 10^{-5} M).

Perylene bisimide **1** is well soluble in most organic solvents such as dichloromethane, toluene and THF. The absorption and emission properties of **1** in dilute dichloromethane solution were investigated by UV/Vis and fluorescence spectroscopy, as shown in Figure S1. Perylene bisimide **1** shows strong absorption in visible light region with absorption maxima at 546 nm in CH_2Cl_2 that corresponds to the S_0–S_1 of the perylene core. The absorption from the perylene bisimide core structure and carbazole groups shows their typical characteristics, which indicates that the interaction between them is weak due to the isolation by long alkyl chains. Quite similar to most of the bay-area bis-phenoxy substituted perylene bisimides, it is nice mirror image between the emission and absorption spectra with a Stokes shift of 35 nm. Both of them show vibronic structure in the S_0-S_1 absorption bands, indicating that the electronic transition is coupled with the vibration of the perylene skeleton. The photoluminescence efficiency of **1** in CH_2Cl_2 was determined to be 12% that is lower than that of the reported similar compound with absence of carbazole groups. The relatively lower efficiency might be attributed to fluorescence quenching by photoinduced electron transfer processes from carbazole to perylene bisimide core through space.

4. Electrochemical properties of compound 1

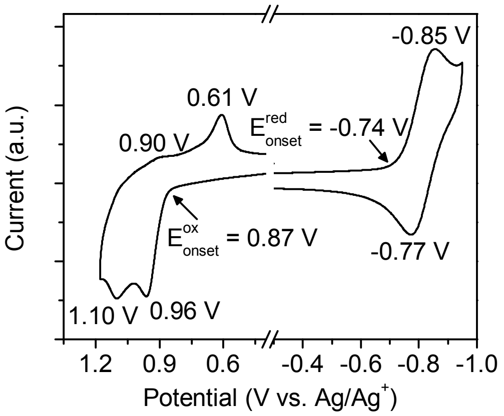

Figure S2. Cyclic voltammograms of compound **1** at room temperature, 0.1 M $TBAPF_6$ in CH_2Cl_2 / acetonitrile (positive), DMF (negative), scan rate 50 mV·s^{-1}.

Table S1. Redox properties of carbazole-functionalized perylene bisimide **1** (vs. Ag/Ag$^+$).

E_{ox}(onset)	E_{red}(onset)	E_{ox1}(irrev.)	E_{ox2}(irrev.)	E_{I}(PBI/PBI$^-$)	HOMO[a]	LUMO[b]	E_g^{CV}	E_g^{opt}[c]
(V)	(V)	(V)	(V)	(V)	(eV)	(eV)	(eV)	(eV)
0.87	-0.74	0.96/0.61	1.10/0.90	-0.85/-0.77	-5.46	-3.94	1.52	2.14

[a] HOMO energy level was calculated using the oxidation onset potential measured in CH_2Cl_2 / acetonitrile (glass carbon electrode with 0.1 M $TBAPF_6$ as the supporting electrolyte). The voltage is referenced to an Ag/Ag$^+$ standard.

[b] LUMO energy level was calculated using the reduction onset potential measured in DMF. The energy level of the ferrocene (Fc) reference (4.8 eV) was calibrated by measuring the cyclic voltammogram of Fc in corresponding solution.

[c] The optical band gap was calculated using the equation $E_g^{opt} = 1240 \times \lambda_{edge}^{-1}$, where λ_{edge} is the onset value of the absorption spectrum of the dichloromethane solution in the direction of longer wavelength.

The redox properties of compound **1** were investigated by cyclic voltammetry (Figure S2) and the redox data are summarized in Table S1. The LUMO that locates at the perylene bisimide core was determined to be -3.94 eV calibrated by ferrocene energy level (-4.8 eV). The first oxidation signal of compound **1** appeared at 0.87 V that corresponds to the formation of carbazyl radical cation, from which the HOMO that locates at carbazole groups was determined to be -5.46 eV. The energy gap between the HOMO and LUMO levels determined by cyclic voltammetry was 1.52 eV, which is much smaller than the energy gap between the oxidation and reduction potential of perylene bisimide core that is 2.14 eV calculated from the oneset position in the absorption spectrum of compound **1**. Thus, we can certainly conclude that the first oxidation potential of carbazole groups must be lower than that of perylene bisimide core. The difference between the oxidation potential of carbazole groups and perylene bisimide core demonstrates that the perylene bisimide core will not be affected during the electrochemical polymerization process within the potential range used in our experiments (-0.5 V – +0.90 V).

5. AFM images of bare ITO and ECP layer of three scanning cycles

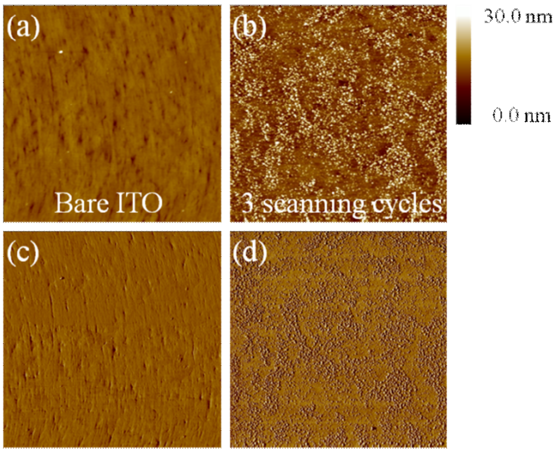

Figure S3. AFM height images and phase images of bare ITO (a, c) and ECP layer of three scanning cycles (b, d). The size of the images is 5μm×5μm, and Z scale is 30 nm. The ultra-thin layers were prepared by ECP method under the conditions as: 0.5 mg·mL^{-1} **1**, 0.1M TBAPF$_6$, scanning potential region − 0.50 — + 0.90 V, mixed solvents V_{CH2Cl2} : V_{CH3CN} = 3:2, scanning rate 400 mV·s^{-1}.

Through comparing the AFM images and phase images of bare ITO and ECP layer of three scanning cycles, ITO has one phase and ECP layer has two phases, we can conclude that the "domain" is due to the ECP layer coating，not the ITO itself.

6. Stability and insolubility of ECP Film in chlorobenzene

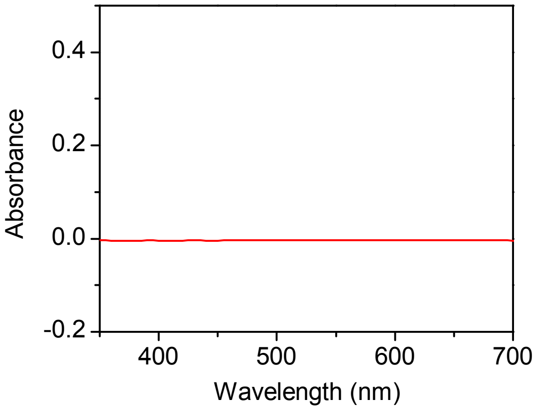

Figure S4. The absorption spectrum of solvent chlorobenzene (the solvent dissolving PCDTBT and $PC_{71}BM$ for device fabrication) after rinsing the pristine electrochemical cross-linked film.

We rinsed the pristine electrochemical cross-linked film with chlorobenzene (the solvent dissolving PCDTBT and $PC_{71}BM$ for device fabrication) and measured the absorption spectrum of rinsing solvent, finding that there was no absorption of perylene bisimide, which can confirm the stability and insolubility of electrochemical cross-linked film in organic solvents.

7. UPS measurement of ITO and ECL

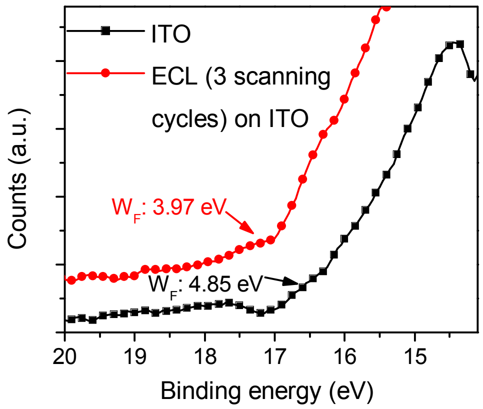

Figure S5. UPS spectra of ITO and ECL (3 scanning cycles) on ITO (He 1α, hν = 21.2 eV) referred to the Fermi level of the spectrometer at zero binding energy. W_F were calculated by using the formula: $W_F = 21.2 - Eb_{onset}$.

8. The effect of the ECP layers on the light transmission property

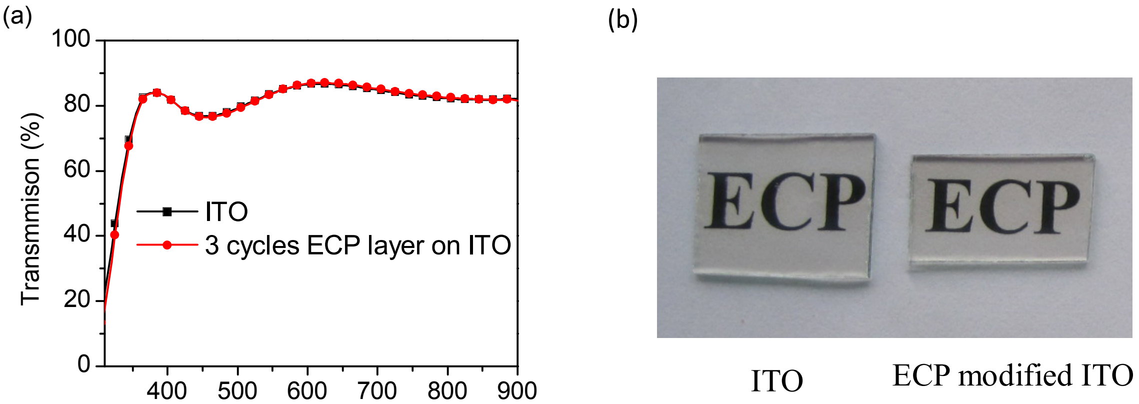

ITO

ECP modified ITO
(3 scanning cycles)

Figure S6. (a) The transmission spectra of ITO and the electrochemical cross-linked domain-like ultra-thin layer of three CV scanning cycles. (b) The photos of ITO (left) and electrochemical cross-linked domain-like ultra-thin layer of three CV scanning cycles (right) under natural light (the black characters were printed on a white paper).

There is little difference between the transmission spectra of ITO and the electrochemical cross-linked domain-like ultra-thin layer of three CV scanning cycles, which demonstrates that there is little influence of the ECP layers on the light transmission property of the device.

9. EIS measurement of bare ITO and ECP layers

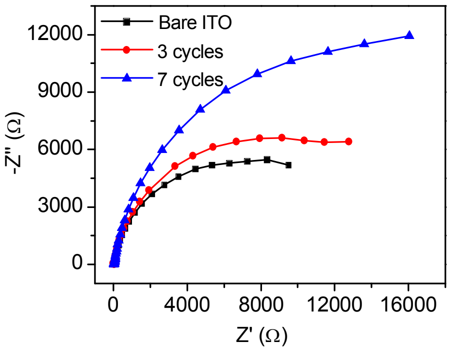

Figure S7. The Electrochemical Impedance Spectroscopy (EIS) of bare ITO and cross-linked domains of different CV scanning cycles.

The resistance of cross-linked domains modified ITO increases with the increasing of CV scanning cycles, which demonstrates that the less conductivity of cross-linked domains with higher density.

10. Dark conductivity property of inverted OPV cell

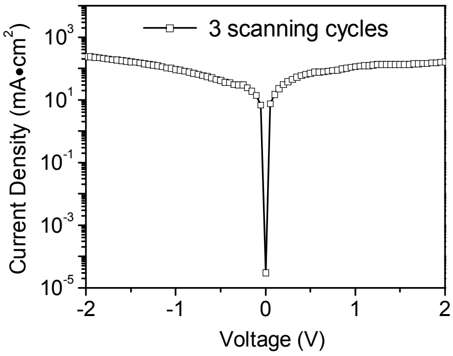

Figure S8. *J–V* characteristic with inverted device structure of ITO/ECL (3 scanning cycles) /PCDTBT: $PC_{71}BM$ (90 nm)/MoO_3 (10 nm)/Al (100 nm) in the dark.

In dark, the device with inverted device structure of ITO/ECL (3 scanning cycles) /PCDTBT: $PC_{71}BM$ (90 nm)/MoO_3 (10 nm)/Al (100 nm) showed a high leakage current and a low rectification ratio, which indicates the device needs to be further optimized.